

Chapter 8

Optical Remote Sensing for Characterizing the Spatial Distribution of Stack Emissions

Michel Grutter¹, Roberto Basaldud¹, Edgar Flores¹, and Roland Harig²

Abstract In this contribution, optical methods based on passive FTIR (Fourier Transform Infrared) and DOAS (Differential Optical Absorption Spectroscopy) techniques have been used to characterize the dispersion of gas emissions from industrial sources. Portable, zenith-looking, passive-DOAS instruments measured the horizontal distribution of an SO₂ plume from a power plant in a coastal town of Mexico. The column density of this gas was measured while making traversals across the plume with a car and a boat downwind from the emission source. The cross sections measured at different distances from the source are used to characterize the horizontal dispersion and to estimate emission fluxes. In addition, a Scanning Infrared Gas Imaging System (SIGIS) was used to acquire passive IR spectra at 4 cm⁻¹ resolution in a two-dimensional array, from which a false-color image is produced representing the degree of correlation of a specific gaseous pollutant. The 24-h, real-time animations of the SO₂ plume help us to understand dispersion phenomena in various atmospheric conditions. The wealth of information retrieved from these optical remote sensors provides an alternative method for evaluating the results from plume dispersion models.

Keywords: Industrial emissions, optical remote sensing, passive DOAS, passive FTIR, plume dispersion

8.1 Introduction

The dispersion of atmospheric pollutants from stacks is often characterized by mathematical models which predict the ground-level concentrations from meteorological, topographical and emission data. Tall stacks do not eliminate the

¹ *Centro de Ciencias de la Atmósfera, Universidad Nacional Autónoma de México, 05410 México D.F. México*

² *Institut für Messtechnik, Technische Universität Hamburg-Harburg, 21079 Hamburg, Germany*

pollution to the atmosphere, but they do aid in reducing ground-level concentrations and their potentially harmful or damaging effects (Schnelle and Partha 2000). The tall stack, however, may not always provide the best solution when the atmospheric conditions do not favor long range dispersion. The most widely used models for regulatory purposes are the deterministic Gaussian plume models. The performance of such models is commonly evaluated by experimentally determining the concentration of a pollutant at a number of receptor points and comparing the measurements with the model output. This task can be expensive, time consuming and the results may not represent the general performance of the model over the total area of interest.

In this contribution, we demonstrate how measurements, based on optical remote sensing, are used to characterize the spatial distribution of stack emissions. The plume's structure is determined by two methods based on the radiative absorption and emission of the polluting gases. The first technique measures the amount of absorption of solar UV by molecules like SO_2 and NO_2 . The radiation is spectroscopically analyzed so that the column concentration of these gases can be monitored while moving along a path perpendicular to the propagation of the plume. This measurement is a cross-section of the **horizontal distribution** of the plume at a specific distance from the source. The second technique uses a spectroscopic analysis of the natural thermal radiation from the plume and surroundings. These thermal emissions are analyzed with a passive infrared sensor and used to identify the characteristic emission/absorption properties of specific constituents in the plume. A two-dimensional image of the **vertical distribution** of the plume is constructed by scanning the area around the emission source.

The two measurement techniques were implemented in Manzanillo, a coastal town with 138,000 inhabitants (INEGI 2005), located on the Pacific coast of Mexico, in the State of Colima (19.03N, 104.19W). A large, oil-fired power plant, with a maximum capacity of producing 1,900MW of electricity, is located approximately 3 km south of the town center. The oil used in this plant has a high content of sulphur (3–4%) such that the plume produced during combustion is high in SO_2 . In the following sections, the measurement techniques will be described and selected results will be presented.

8.2 Passive DOAS

The Differential Optical Absorption Spectrometer (DOAS) is a widely used technique for the continuous measurement of atmospheric gases (Platt 1994; Platt et al. 1979). In its configuration for active sensing, where the light traveling along an open path is provided by a synthetic radiation source, low detection limits for the ambient concentrations of various gases (O_3 , SO_2 , HCHO, NO_2 , several hydrocarbons, aromatic compounds, etc.) can be achieved. This technique is based on the spectral analysis of the differential absorption by molecules in the ultraviolet and visible part of the spectrum. The broader extinction of UV light due to other

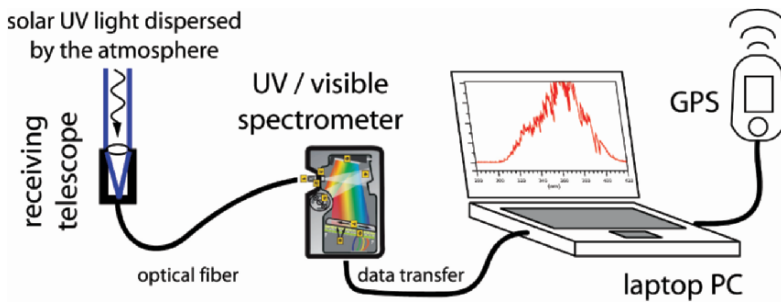


Fig. 8.1 Schematic diagram of the portable passive DOAS instrument used for measuring column gas concentrations on a moving platform

processes such as dispersion by fine particles is cancelled when processed and thus not taken into account.

In the passive sensing configuration, as is in the case when dispersed light from the sun (i.e. from a blue sky) is used as the radiation source, the spectral analysis is based on the differential absorption of a particular gas or group of gases. The total amount of molecules in an atmospheric column is determined between the altitude where the radiation is dispersed and the position of the observer. These techniques have been used to identify and quantify atmospheric gases both in industrial (Lohberger et al. 2004) and volcanic (Bobrowski et al. 2003; Lee et al. 2005) plumes.

The scheme used for making passive DOAS measurements in this study is presented in Fig. 8.1. The dispersed solar UV light is collected with a narrow field-of-view (<20 mrad) telescope that was built in-house. This consists of a concave lens ($f = 100$ mm), a bandpass optical filter (240–400 nm) and a 200- μ m diameter optical fiber. The light is analyzed with a hand-held spectrometer (Ocean Optics, model S2000), at a resolution of 0.44 nm between 280 and 420 nm. This device uses a UV holographic grating, a 2048 element CCD detector and has no moving parts; hence, it is appropriate for this type of application. The spectra are recorded using an interface based on LabView that couples each acquisition with a longitude-latitude fix from a GPS receiver. User defined parameters along with dark and background spectra are entered prior to each measurement along a trajectory.

The spectra are evaluated following these general steps:

- Reference spectra of the target gases are generated for each spectrometer through the convolution of a high-resolution reference spectrum from the literature or a spectral library. For this purpose the instrumental line shape (ILS), determined by measuring the emission line from a low-pressure mercury lamp, is used to produce a reference spectrum with the true resolution of the spectrometer.
- A dark spectrum is subtracted from the measured spectrum (blue trace in Fig. 8.2) to correct the baseline offset.

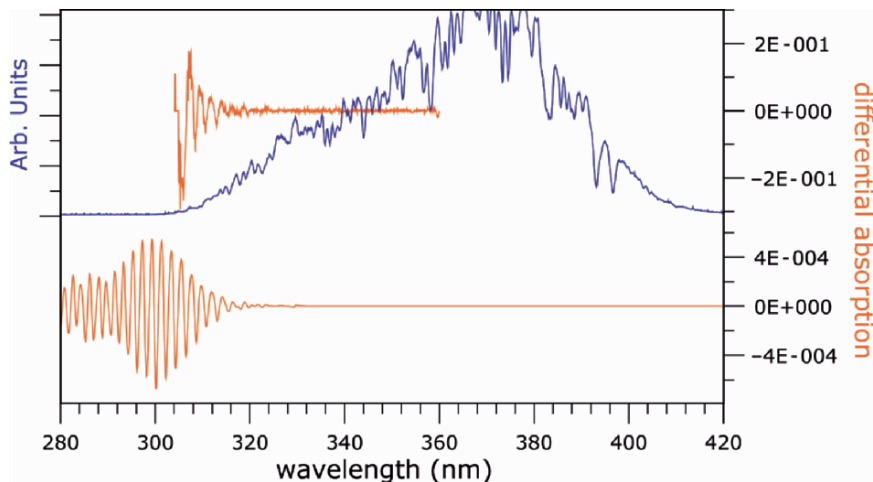


Fig. 8.2 Measured spectrum (blue trace) from solar dispersed light in the direction of the zenith and across a plume. The orange traces are differential absorptions of SO_2 from the measurement (upper) and from the reference (lower) spectra

- A differential absorption spectrum (upper orange trace in Fig. 8.2) is created from the background spectrum measured outside the gas plume and by applying a high-pass filter.
- The resulting spectrum is fitted to the reference spectrum (lower trace) using the software DOASIS (Kraus 2003).
- SO_2 is analyzed by fitting the reference (Vandaele et al. 1994) in the region 306–317 nm and taking into account the interference of O_3 absorptions. NO_2 (Harder et al. 1997) is evaluated in the 350–390 nm region.

Figure 8.3 presents the results from traversals of a plume over the ocean made from a small boat that sailed across the Manzanillo Bay. Fig. 8.3a is a map of the region with the red dot marking the power plant location. The trajectory of the boat is drawn on the map as a thick black line starting close to the location marked by the green star and moving in the direction marked by the arrows. The positions of the plume crossings are shown on the boat trajectory in false colors whose scale is given in the same figure. The wind rose in Fig. 8.3b shows that winds were predominately from the southeast, coinciding with the positions where the plume was detected.

Figure 8.3c is a plot of the SO_2 column concentration along the trajectory of the boat. The first large peak in this plot represents the first pass below the plume at 2.5 km (in a straight line) downwind of the source. The SO_2 profile reveals that the width of the plume at this distance was 1,250 m, which can be interpreted as its horizontal dispersion profile. The second and forth passes, approximately 5 km from the emission source, have widths of 1,500 m. The third pass and furthest from the source (10 km) had an approximate width of 2,800 m.

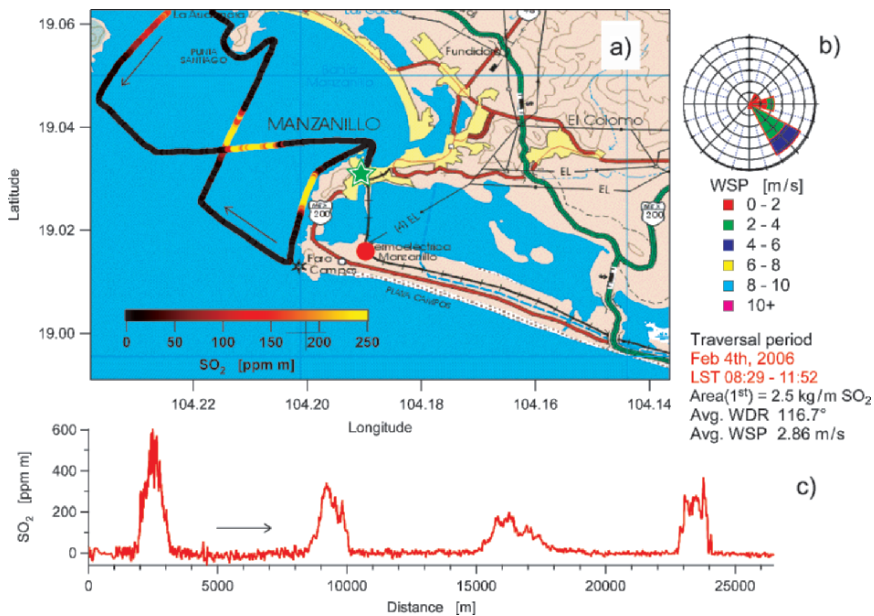


Fig. 8.3 The passive-DOAS measurements shown here characterize the spatial distribution of the SO₂ in a plume from a power plant (red dot) in Manzanillo, Mexico. In this figure are **a.** the map of the region with the boat trajectory, **b.** the wind chart and **c.** the column SO₂ concentration measured along this path

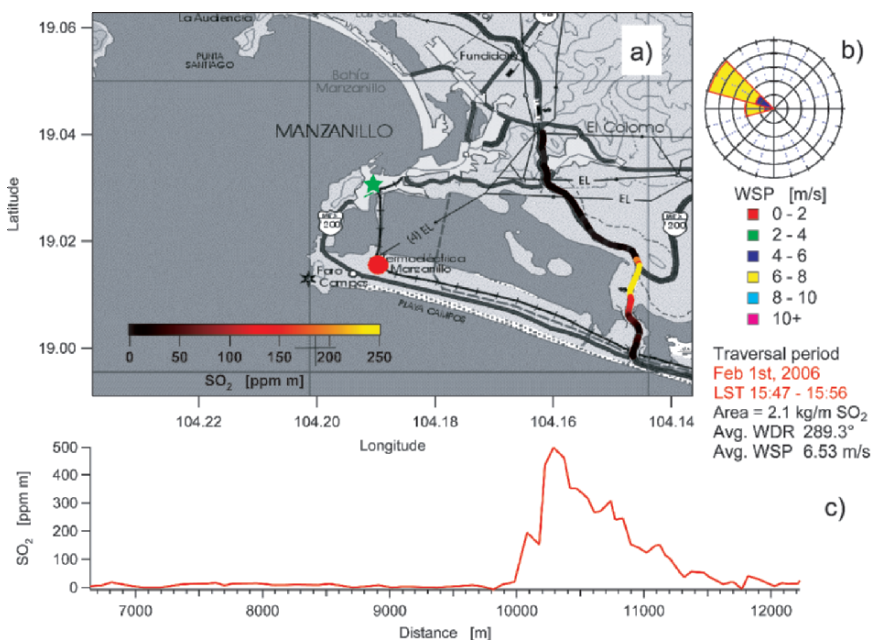


Fig. 8.4 Results from a passive-DOAS measurement done from the land along a roadway east from the power plant (red dot) in Manzanillo, Mexico. Frame **a.** is a map with the boat trajectory, **b.** is the wind chart and **c.** is the column SO₂ measured along this path

Traversals of the plume with the passive DOAS were more often done on land while driving a car along a highway. One of the many measurements done during the one-week period of the campaign is presented in Fig. 8.4. Here the wind was coming from the WNW as often occurred during the afternoon. The plume was carried across the lagoon and measured by the instrument, as can be seen in Fig. 8.4a, c. The peak concentration was registered at a distance of 7.7 km from the emission source and, according to the SO_2 profile, its width was $\sim 1,500$ m.

In addition to providing the horizontal distribution of the plume, these profiles were used to estimate the emission fluxes of SO_2 and NO_2 . This is done by conversion to units in kg/m^2 and integrating under the curve. The resulting values are multiplied by the wind speed measured at a 15 m tower close to the emission source.

8.3 Passive FTIR

8.3.1 Radiative Transfer Model

Passive remote sensing of gas clouds is based on the analysis of infrared radiation absorbed and emitted by the molecules in the clouds. The propagation of radiation through the atmosphere is described by radiative transfer theory. One method for modeling the radiative transfer is the division of the atmosphere along the optical path into layers which are assumed to be homogeneous with regard to all physical and chemical properties. Each of these layers absorbs a fraction of the radiation entering the layer but also emits radiation. Both of these processes depend on the properties of the layer, such as composition, temperature and pressure.

In order to model the radiation from the sky, many layers are required due to the different temperatures and pressures at different altitudes. However, to describe the basic spectral characteristics of a gas cloud in the lowest layer of the atmosphere, as measured by a ground-based passive infrared spectrometer, a model with only two layers and a background is sufficient in most cases. As shown in Fig. 8.5, radiation from the background, e.g., a surface, propagates through the gas cloud (Layer 2) and the atmosphere between the cloud and the spectrometer (Layer 1). Layers 1 and 2 are considered homogeneous with regard to all physical and

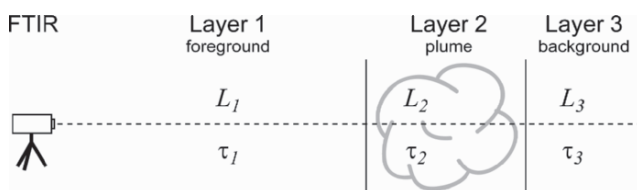


Fig. 8.5 Simple radiative transfer model for the identification of gas pollutants from passive infrared spectra

chemical properties within each layer. The radiation containing the signatures of the atmosphere, the gas cloud, and the background radiation is measured by the spectrometer.

In this model, the spectral radiance at the entrance aperture of the spectrometer L_1 can be described by

$$L_1 = (1 - \tau_1)B_1 + \tau_1 [(1 - \tau_2)B_2 + \tau_2 L_3], \quad (1)$$

where τ_i is the transmittance of layer i , B_i is the spectral radiance of a blackbody at the temperature T_i of layer i , and L_3 is the radiance that enters the layer of the cloud from the background. All quantities in Eq. 1 are frequency dependent. If the background of the field of view is a surface, the radiation entering the cloud contains radiation emitted by the surface and reflected radiation, i.e., ambient radiation and radiation from the sky. The contribution of scattering is in this case neglected.

If the temperatures of the Layers 1 and 2 are equal ($B_1=B_2$), Eq. 1 can be simplified to:

$$L_1 = B_1 + \tau_1 \tau_2 (L_3 - B_1). \quad (2)$$

The radiance difference $\Delta L = L_1 - L_3$ is given by

$$\Delta L = (1 - \tau_1 \tau_2) \Delta L_{13}, \quad (3)$$

where $\Delta L_{13} = B_1 - L_3 = B_2 - L_3$. In this work the term ‘‘radiance’’ is used as a simplifying synonym for the correct term ‘‘spectral radiance.’’ Thus, the analysis of the spectrum allows detection, identification, and quantification of the species contained in the gas cloud.

8.3.2 Method for the Detection of SO_2

In the present work, the passive FTIR technique is used to examine the plume shape from a power plant based on the identification of SO_2 under the influence of different meteorological conditions. The detection method is based on the approximation of a measured spectrum by reference spectra, which has been described elsewhere (Harig and Matz 2001; Harig et al. 2002). First, the spectrum of the brightness temperature $T_{br}(\sigma)$ is calculated. The detection is performed in three steps. In the first step, the mean brightness temperature is subtracted and the signatures of the target compound (SO_2) and atmospheric species (H_2O , O_3) are fitted to the resulting spectrum. Moreover, the baseline is approximated by a least-squares fit. In the next step, the contributions of all fitted signatures (i.e. atmospheric species and baseline) except the signature of the target compound (SO_2 in this case) are subtracted from the measured spectrum. In the final step, the

coefficient of correlation between the corrected spectrum, i.e., the result of the subtraction, and a reference spectrum in a specific spectral range, is calculated. The calculation is performed for three different column densities of the target compound. The maximum value for this coefficient is used as an indicator for the presence of the gas, as shown by the lighter colors in Fig. 8.7.

Reference spectra with different column densities are calculated by convolution of high-resolution transmittance spectra (e.g., calculated with absorption coefficients computed using HITRAN/FASCODE (Rothman et al. 2003; Smith et al. 1978) with a real instrument line shape function (Harig 2004)).

8.3.3 Scanning Infrared Gas Imaging System

SIGIS (Scanning Infrared Gas Imaging System) is an imaging remote sensing system based on the combination of an interferometer with a single detector element and a scanning mirror. The system is comprised of the interferometer OPAG 22 (Bruker Daltonics, Leipzig, Germany), a telescope, an azimuth-elevation-scanning mirror actuated by stepper motors, a data processing and control system with a digital signal processor (FTIR DSP), an image processing system (Video DSP), a video camera and a PC for control and display of the results (Fig. 8.6).

The maximum optical path difference of the interferometer configuration used in this work is 1.8 cm, resulting in a spectral resolution of approximately 0.5 cm^{-1} . For the visualization of gas clouds, however, a spectral resolution of 4 cm^{-1} is used. The choice of resolution has been evaluated as a good trade-off between the goals of a low detection limit, sufficient selectivity and a short measurement time. The signal-to-noise ratio improves with decreasing spectral resolution for a constant

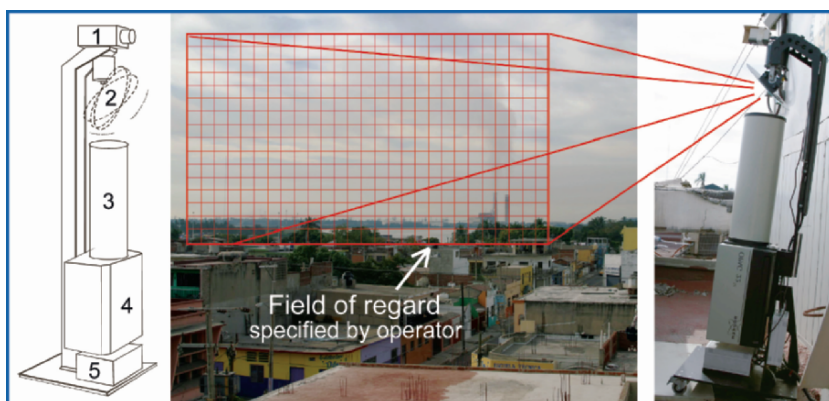


Fig. 8.6 Schematic diagram (left) and photograph (right) of the Scanning Infrared Gas Imaging System (SIGIS), with (1) video camera, (2) azimuth-elevation-scanning mirror, (3) telescope, (4) spectrometer and (5) DSP system. The field of regard is illustrated in the center

measurement time (Harig 2004). On the other hand, higher resolution yields higher selectivity. At 4 cm^{-1} , six two-sided interferograms per second can be measured.

For the visualization of pollutant clouds, the scanning mirror is sequentially positioned to an array of points within the field of regard. The size and the direction of the field of regard and the spatial resolution (i.e. the angle between adjacent fields of view) are variable. Each interferogram measured by the interferometer is recorded by the FTIR DSP system. The Fourier transformation is performed by the DSP, the spectrum is transferred to the PC and analyzed using the identification method described in section 8.3.2. The results are visualized by overlaying the false color images to a video image. For each target compound in the spectral library, various false color images visualizing the results of the detection, identification and quantification algorithms are produced. The SO_2 molecule was found to be a good tracer for the visualization of the emission plume due to its high abundance in this particular case, although a great variety of gases can be used as identifiers in other applications. Simultaneous with the analysis and visualization of one interferogram by the FTIR DSP and the PC, the scanning mirror is set to the following position to record the next interferogram, and so on.

8.3.4 Measurements

The instrument was placed on the roof of a 3-story building in downtown Manzanillo. The location, that was 2.5 km north of the power plant, is marked by a green star in Figs. 8.3a and 8.4a. Various images of the exhaust gas plume of the plant were recorded. The images in Fig. 8.7 are taken from an 8-h sequence, which captured the SO_2 distribution around the source during distinctly different atmospheric conditions. The coefficient of correlation between the measured and processed spectra and a reference spectrum of SO_2 is shown as a false color representation (as described in section 8.3.2) and superimposed on the video image. A complete scan was made every 3 min from which the evolution of the plume can be followed in detail. The eight images shown in Fig. 8.7 demonstrate the large variability in the spatial distribution of SO_2 during an eight and a half hour period.

It is evident from this particular example that the westerly sea breeze pushes the power plant's pollution towards the land throughout the afternoon with some deviations as seen in the 15:17 frame. At around 20:00 hours, the wind direction changes and the land breeze begins to dominate. Particularly interesting is that when the plume has already changed its direction towards the sea as can be seen in the 21:06 frame, an air mass which had been collecting pollution over the land within the last several hours passes the observation window from left to right (shown as the red area at the left in the 21:06 frame). This can be more clearly seen in a video animation which was created for the interpretation. The easterly land breeze then predominates throughout the night as shown in the last frame of Fig. 8.7.

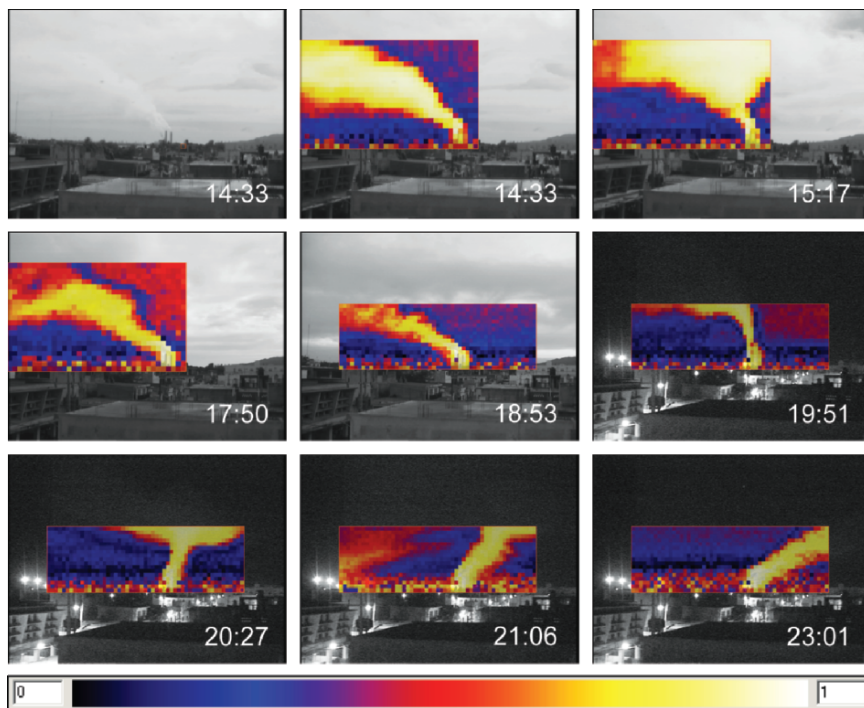


Fig. 8.7 Sequence of video and SIGIS images showing the SO_2 distribution on Feb 2, 2006 in Manzanillo, Mexico. The local time is given on the bottom right

8.4 Conclusions

The results presented here show how the spatial distribution of the gaseous pollutants from an industrial emission source can be measured with optical remote sensors. The passive DOAS instrument was successful in obtaining horizontal profiles of the plume by making transects perpendicular to the plume's axis and at different distances from the source. From these measurements, that were performed both from sea and land, indirect estimates of the emission fluxes can be obtained. Similarly, the temporal evolution of the horizontal and vertical plume structure was continuously measured with a passive FTIR instrument, which is capable of detecting pollutants from distances greater than 2.5 km from the source. The Scanning Infrared Gas Imaging System can continuously register two-dimensional images of gaseous species which allows the monitoring and animation of fundamental plume propagation properties (degree of dispersion, direction, speed, etc.) not only during the day but also quite impressively during the night.

This contribution describes two state-of-the-art methodologies which can contribute to the field of advanced environmental monitoring with their ability to

detect and visualize clouds of potentially toxic pollutants from a distance. Additionally, the measurement of the spatial distribution of emission source with these techniques can be used as an alternative and convenient way to evaluate the performance of plume dispersion models commonly used to diagnose these situations. Finally, given the potential effects which the emissions of large quantities of pollutants have on global climate and the health of humans, plants and the ecosystems, one cannot underestimate the need to reduce the emissions by exploiting newer and better technologies.

Acknowledgements This work has been funded through project CONACYT-CFE-2004-C01-44. The authors would like to thank Stefan Kraus and the University of Heidelberg for making the software DOASIS available, the M. in. Sc. student Andrés Hernández and the personnel at the Environmental Protection Department from CFE in Manzanillo for their valuable help during the field campaign and the mechanical workshop (M.A. Meneses and A. Rodriguez) at CCA-UNAM for helping build part of the instruments.

References

- Bobrowski N., Hönninger G., Galle B., and Platt U. (2003), Detection of bromine monoxide in a volcanic plume, *Nature*, 423, 273–276.
- Harder J.W., Brault J.W., Johnston P.V., and Mount G.H. (1997), Temperature dependent NO₂ cross sections at high spectral resolutions, *J. Geophys. Res.*, 102(D3), 3861–3880.
- Harig R. (2004), Passive remote sensing of pollutant clouds by FTIR spectrometry: Signal-to-noise ratio as a function of spectral resolution, *Appl. Opt.*, 43(23), 4603–4610.
- Harig R. and Matz G. (2001), Toxic cloud imaging by infrared spectroscopy: A scanning FTIR system for identification and visualization, *Field Anal. Chem. Technol.*, 5(1–2), 75–90.
- Harig R., Matz G., and Rusch P. (2002), Scanning Infrared Remote Sensing System for Identification, Visualization, and Quantification of Airborne Pollutants, *Proc. SPIE*, 4575, 83–94.
- INEGI. Censo de población y vivienda 2005, Instituto Nacional de Estadística Geográfica e Informática, 2005.
- Kraus S. *DOAS Intelligent System*, University of Heidelberg in cooperation with Hoffman Messtechnik GmbH, 2003.
- Lee C., Kim Y.J., Tanimoto H., Bobrowski N., Platt U., Mori T., Yamamoto K., and Hong C.S. (2005), High ClO and ozone depletion observed in the plume of Sakurajima volcano, Japan, *Geophys. Res. Lett.*, 32, L21809.
- Lohberger F., Hönninger G., and Platt U. (2004), Ground-based imaging differential optical absorption spectroscopy of atmospheric gases, *Appl. Opt.*, 43, 4711–4717.
- Platt U. (1994), Differential optical absorption spectroscopy (DOAS). (In M.W. Sigrist (Ed), *Air monitoring by spectroscopy techniques* (pp. 27–83), Wiley Interscience, New York).
- Platt U., Perner D., and Pätz H.W. (1979), Simultaneous measurement of atmospheric CH₂O, O₃ and NO₂ by differential optical absorption, *J. Geophys. Res.*, 84, 6329–6335.
- Rothman, L.S., Barbe A., Benner D.C., Brown L.R., Camy-Peyret C., Carleer M.R., Chance K., Clerbaux C., Dana V., Devi V.M., Fayt A., Flaud J.-M., Gamache R.R., Goldman A., Jacquemart D., Jucks K.W., Lafferty W.J., Mandin J.-Y., Massie S.T., Nemtchinov V., Newnham D.A., Perrin A., Rinsland C.P., Schroeder J., Smith K.M., Smith M.A.H., Tang K., Toth R.A., Vander Auwera J., Varanasi P., and Yoshino K. (2003), The HITRAN molecular spectroscopic database: edition of 2000 including updates through 2001, *J. Quant. Spectrosc. Radiat. Transfer*, 82, 5–44.

- Schnelle K.B. and Partha R.D., *Atmospheric Dispersion Modeling Compliance Guide*, (McGraw-Hill, New York, 2000).
- Smith H.J.P., Dude D.J., Gardner M.E., Clough S.A., Kneizys F.X., and Rothman L.S. FASCODE- Fast Atmospheric Signature Code (Spectral Transmittance and Radiance), pp. Report AFGL-TR-78-0081, Air Force Geophysics Laboratory Technical, Hanscom AFB, MA., 1978.
- Vandaele A.C., Simon P.C., Guilmot J.M., Carleer M., and Colin R. (1994), SO₂ absorption cross section measurement in the UV using a Fourier transform spectrometer, *J. Geophys. Res.*, 99, 25599.